Examination of the Pyridine Binding to the Bifunctional Lewis Acid B,B′-Diphenyldiboradiferrocene

Thilagar Pakkirisamy,[†] Krishnan Venkatasubbaiah,[†] W. Scott Kassel,[§,#] Arnold L. Rheingold,[§] and Frieder Jäkle*[,†]

Department of Chemistry, Rutgers University−Newark, 73 Warren Street, Newark, New Jersey 07102, and University of California, San Diego, La Jolla, California 92093

Received February 21, 2008

The binding behavior of the bifunctional Lewis acid (η^5-$C_5H_5Fe)_2[\mu$-$(C_5H_3(BPh))_2]$ (**3**) toward different pyridine derivatives as the Lewis base has been investigated. The 1:1 and 1:2 adducts, **3**·D and **3**·D_2 (donor, D = 4-*tert*-butylpyridine (*t*Bupy) and 4-dimethylaminopyridine (DMAP)), were obtained by low-temperature crystallization or slow solvent evaporation techniques. The complexes were fully characterized by multinuclear NMR, IR, and elemental analysis. Single-crystal X-ray diffraction data were collected for the 1:1 adduct with DMAP and for both 1:2 adducts, and the marked structural changes upon pyridine binding are discussed in detail. In solution, the 1:2 adducts were found to readily undergo dissociation with formation of the 1:1 adducts as the dominant species at room temperature. Variable-temperature NMR and UV−visible titration studies demonstrate that the first binding process is more than 5 orders of magnitude more favorable than the second binding process.

Introduction

Bifunctional organoboranes are widely studied as receptors for neutral and anionic substrates and as Lewis acid activators for various organic and organometallic reactions.[1,2] They also have attracted considerable interest as building blocks for the preparation of new electronically interesting materials.[3,4]

The use of metallocenes as a redox-active backbone has recently been investigated, and several examples of this intriguing class of bifunctional Lewis acids are worth noting.[2,3,5] The formation of reversible ansa-bridges through intramolecular Lewis acid−base bonding and the assembly of coordination polymers through intermolecular Lewis acid−base interactions have been demonstrated by Wagner and co-workers for 1,1′-diborylferrocenes (**1**, M = Fe(II)).[6–8] Jutzi and co-workers introduced a trinuclear gallium-bridged ferrocenophane [{Fe(η^5-$C_5H_4)_2\}_3Ga_2$] and studied the electronic properties, coordination behavior, and incorporation into polymeric materials.[9] Aldridge and co-workers demonstrated the use of 1,1′-diborylated ferrocenes for fluoride sensing applications.[10] Related diborylcobaltocenium complexes (**1**, M = Co(III)) have been reported by Herberich and co-workers to form an ansa-bridge between the Cp rings upon anion binding.[11] We have investigated the binding properties of ferrocene-based heteronuclear bidentate

* To whom correspondence should be addressed. E-mail: fjaekle@rutgers.edu.
† Rutgers University Newark.
§ University of California, San Diego.
# Current address: Department of Chemistry, Villanova University, 800 Lancaster Ave., 215D Mendel Science Center, Villanova, PA 19085.

(1) (a) Vaugeois, J.; Simard, M.; Wuest, J. D. *Coord. Chem. Rev.* **1995**, *145*, 55–73. (b) Piers, W. E.; Irvine, G. J.; Williams, V. C. *Eur. J. Inorg. Chem.* **2000**, *10*, 2131–2142. (c) Hoefelmeyer, J. D.; Schulte, M.; Tschinkl, M.; Gabbaï, F. P. *Coord. Chem. Rev.* **2002**, *235*, 93–103. (d) Dembitsky, V. M.; Abu Ali, H.; Srebnik, M. *Appl. Organomet. Chem.* **2003**, *17*, 327–345. (e) Wedge, T. J.; Hawthorne, M. F. *Coord. Chem. Rev.* **2003**, *240*, 111–128. (f) Melaïmi, M.; Gabbaï, F. P. *Adv. Organomet. Chem.* **2005**, *53*, 61–99.

(2) Jäkle, F. In *Group 13 Chemistry: From Fundamentals to Applications*; Shapiro, P. J., Atwood, D., Eds.; ACS: Washington, DC, 2002; Chapter 7.

(3) Ma, K.; Scheibitz, M.; Scholz, S.; Wagner, M. *J. Organomet. Chem.* **2002**, *652*, 11–19.

(4) (a) Ding, L.; Ma, K. B.; Durner, G.; Bolte, M.; de Biani, F. F.; Zanello, P.; Wagner, M. *J. Chem. Soc., Dalton Trans.* **2002**, *156*, 6–1573. (b) Heilmann, J. B.; Scheibitz, M.; Qin, Y.; Sundararaman, A.; Jäkle, F.; Kretz, T.; Bolte, M.; Lerner, H.-W.; Holthausen, M. C.; Wagner, M. *Angew. Chem., Int. Ed.* **2006**, *45*, 920–925. (c) Jaska, C. A.; Emslie, D. J. H.; Bosdet, M. J. D.; Piers, W. E.; Sorensen, T. S.; Parvez, M. *J. Am. Chem. Soc.* **2006**, *128*, 10885–10896. (d) Jaska, C. A.; Piers, W. E.; McDonald, R.; Parvez, M. *J. Org. Chem.* **2007**, *72*, 5234–5243.

(5) (a) Examples of binding studies with organoboranes containing other pendant transition metal complexes: Matsumi, N.; Chujo, Y.; Lavastre, O.; Dixneuf, P. H. *Organometallics* **2001**, *20*, 2425–2427. (b) Lee, M. H.; Gabbai, F. P. *Inorg. Chem.* **2007**, *46*, 8132–8138. (c) Sun, Y.; Ross, N.; Zhao, S. B.; Huszarik, K.; Jia, W. L.; Wang, R. Y.; Macartney, D.; Wang, S. N. *J. Am. Chem. Soc.* **2007**, *129*, 7510–7511. (d) Zhao, S. B.; McCormick, T.; Wang, S. *Inorg. Chem.* **2007**, *46*, 10965–10967.

(6) (a) Jäkle, F.; Priermeier, T.; Wagner, M. *Organometallics* **1996**, *15*, 2033–2040. (b) Herdtweck, E.; Jäkle, F.; Wagner, M. *Organometallics* **1997**, *16*, 4737–4745. (c) Grosche, M.; Herdtweck, E.; Peters, F.; Wagner, M. *Organometallics* **1999**, *18*, 4669–4672. (d) Dinnebier, R. E.; Wagner, M.; Peters, F.; Shankland, K.; David, W. I. F. *Z. Anorg. Allg. Chem.* **2000**, *626*, 1400–1405.

(7) Fontani, M.; Peters, F.; Scherer, W.; Wachter, W.; Wagner, M.; Zanello, P. *Eur. J. Inorg. Chem.* **1998**, 1453–1465.

(8) Scheibitz, M.; Bolte, M.; Lerner, H. W.; Wagner, M. *Organometallics* **2004**, *23*, 3556–3559.

(9) (a) Jutzi, P.; Lenze, N.; Neumann, B.; Stammler, H.-G. *Angew. Chem., Int. Ed.* **2001**, *40*, 1424–1427. (b) Althoff, A.; Jutzi, P.; Lenze, N.; Neumann, B.; Stammler, A.; Stammler, H. G. *Organometallics* **2003**, *22*, 2766–2774. (c) Althoff, A.; Eisner, D.; Jutzi, P.; Lenze; N.; Neumann, B.; Schoeller, W. W.; Stammler, H. G. *Chem.−Eur. J.* **2006**, *12*, 5471–5480.

(10) (a) Bresner, C.; Aldridge, S.; Fallis, I. A.; Jones, C.; Ooi, L.-L. *Angew. Chem., Int. Ed.* **2005**, *44*, 3606–3609. (b) Aldridge, S.; Bresner, C.; Fallis, I. A.; Coles, S. J.; Hursthouse, M. B. *Chem. Commun.* **2002**, 740–741. (c) Bresner, C.; Day, J. K.; Coombs, N. D.; Fallis, I. A.; Aldridge, S.; Coles, S. J.; Hursthouse, M. B. *Dalton Trans.* **2006**, 3660–3667. (d) Day, J. K.; Bresner, C.; Coombs, N. D.; Fallis, I. A.; Ooi, L.-L.; Aldridge, S. *Inorg. Chem.* **2008**, *47*, 793–804.

(11) (a) Herberich, G. E.; Fischer, A.; Wiebelhaus, D. *Organometallics* **1996**, *15*, 3106–3108. (b) Herberich, G. E.; Englert, U.; Fischer, A.; Wiebelhaus, D. *Organometallics* **1998**, *17*, 4769–4775. (c) Herberich, G. E.; Englert, U.; Fischer, A.; Wiebelhaus, D. *Eur. J. Inorg. Chem.* **2004**, 4011–4020.

10.1021/om8001608 CCC: $40.75
Publication on Web 06/13/2008

Scheme 1. Formation of Adducts 4 and 5 (py = pyridine; *t*Bupy = 4-*tert*-butylpyridine; DMAP = 4-dimethylaminopyridine)

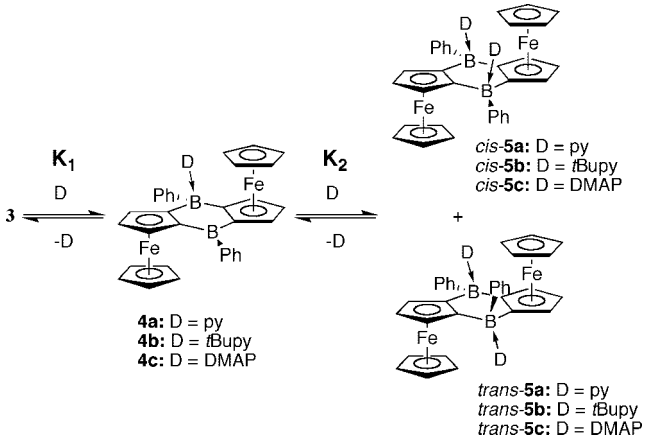

Lewis acids and, for example, successfully applied them as chiral reagents in stereoselective allylation reactions.[12]

Recently, we communicated the synthesis, redox chemistry, and binding properties of an unusual *ortho*-diborylated ferrocene dimer (**3**).[13] A particularly interesting feature of the bifunctional Lewis acid **3** is that the Lewis acidity of the boron centers can be reversibly adjusted through oxidation of the iron centers.[14] Another unusual aspect is that the three-dimensional structure of **3** and consequently the separation of the Fe centers of the ferrocene moieties can be reversibly modified through redox chemistry.[15] An alternative method of modulating the three-dimensional geometry of **3** is through nucleophile binding. Here, we provide full details of the binding properties of **3** toward different pyridine derivatives[16] and the effects on the molecular geometry of the diboradiferrocene framework.

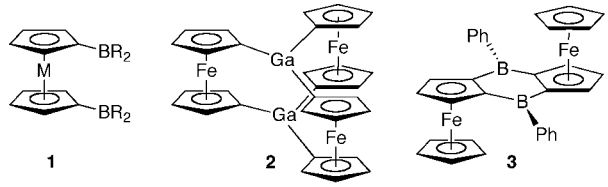

Results and Discussion

Synthetic Aspects. The bifunctional Lewis acid **3** was allowed to react at RT in chlorinated solvents with 2 molar equiv of 4-*tert*-butylpyridine (*t*Bupy) and 4-dimethylaminopyridine (DMAP), respectively (Scheme 1). Compound **5b** was isolated in 88% yield upon evaporation of the solvents and extraction with hexanes, and **5c** was obtained in 77% yield by crystallization from CH_2Cl_2 at −35 °C. For the synthesis of **5a**, compound **3** was dissolved in pyridine and the mixture was kept at −35 °C for 1 day, giving the bis-adduct in 80% yield as an orange crystalline solid. The monocomplexed species **4b** and **4c** were obtained as red crystalline solids in 82% and 80% yield, respectively, by layering of a 1:1 mixture of **3** and the respective pyridine derivatives in CH_2Cl_2 at −35 °C with hexanes. The stoichiometry of the individual adducts was confirmed by ^{1}H NMR integration, elemental analysis, and in the case of **4b**, **5b**, and **5c** single-crystal X-ray diffraction analysis.

Solid State Structures. Orange block-like single crystals of the bis-adduct **5b** were grown by slow solvent evaporation of a 1:2 mixture of **3**/*t*Bupy in chloroform, and needle-like orange crystals of **5c** suitable for X-ray diffraction analysis formed from a mixture of **3** and 2 equiv of DMAP in CH_2Cl_2 at −35 °C. In both cases the *trans*-isomer was obtained selectively upon crystallization. The molecular structures of *trans*-**5b** and *trans*-**5c** are displayed in Figure 1, and selected geometric parameters are provided in Table 1. In both structures, the symmetry equivalence of the ferrocene moieties, phenyl rings, and pyridine ligands, respectively, allows the molecule to reside on a crystallographic inversion center.

Upon pyridine binding, the geometric features of the diboradiferrocene core change dramatically. While for the free acid **3** the central C_4B_2 ring of the bridging dibora-*s*-indacene moiety is significantly tilted toward the CpFe fragments, for *trans*-**5b** and *trans*-**5c** the opposite is true in that the boron centers are bent away from the ferrocene moieties with interplanar angles between the Cp and C_4B_2 rings of 5.5° and 4.2°, respectively (see also Figure 2). This effect can be traced back to the delocalized interaction between the electron-deficient boron centers and the electron-rich iron atoms in **3**,[8,17,18] which is absent in the complexes due to nucleophile binding to the formerly empty p orbital of boron. In addition, steric congestion at boron apparently forces the two ferrocene moieties to bend away from the central C_4B_2 ring.[18] Steric strain upon pyridine binding is further reflected in significant Cp//Cp tilt angles of 5.4° (*trans*-**5b**) and 6.1° (*trans*-**5c**) between the substituted and unsubstituted Cp rings of each of the ferrocene moieties. The B−C bonds are also slightly longer than in **3** due to the hybridization change upon expansion of the coordination sphere to a tetrahedral environment.[19] Consequently, compared to the free acid, the B···B distance increases by 0.175 and 0.193 Å for *trans*-**5b** and *trans*-**5c**, respectively. All these factors ultimately lead to expansion of the molecule and considerably longer Fe···Fe distances of 5.940 and 5.910 Å relative to that of 5.123 Å in **3**. An illustration of these effects is provided in Figure 2.

The B−N distances of 1.652(3) and 1.640(4) Å for *trans*-**5b** and *trans*-**5c**, respectively, are similar to one another and in the range of other B−N bond lengths reported for organoborane pyridine complexes (mean B−N distance from CSD search for $R_3B\cdot Py$: 1.650 Å). They are close to the B−N distances in related ferrocenylborane pyridine adducts such as $Fc_3B\cdot Py$[20] (1.658 Å) and $FcBMe_2\cdot DMAP$[17] (1.670 Å). However, they are longer than for reported pyridine adducts of $B(C_6F_5)_3$ such as $B(C_6F_5)_3\cdot DMAP$[21] (1.604 Å).

(12) (a) Boshra, R.; Sundararaman, A.; Zakharov, L. N.; Incarvito, C. D.; Rheingold, A. L.; Jäkle, F. *Chem.−Eur. J.* **2005**, *11*, 2810. (b) Boshra, R.; Venkatasubbaiah, K.; Doshi, A.; Lalancette, R. A.; Kakalis, L.; Jäkle, F. *Inorg. Chem.* **2007**, *46*, 10174–10186. (c) Boshra, R.; Doshi, A.; Jäkle, F. *Angew. Chem., Int. Ed.* **2008**, *47*, 1134–1137. (d) Boshra, R.; Doshi, A.; Jäkle, F. *Organometallics* **2008**, *27*, 1534–1541.

(13) Venkatasubbaiah, K.; Zakharov, L. N.; Kassel, W. S.; Rheingold, A. L.; Jäkle, F. *Angew. Chem., Int. Ed.* **2005**, *44*, 5428–5433.

(14) Venkatasubbaiah, K.; Nowik, I.; Herber, R. H.; Jäkle, F. *Chem. Commun.* **2007**, 2154–2156.

(15) (a) Venkatasubbaiah, K.; Doshi, A.; Nowik, I.; Herber, R. H.; Rheingold, A. L.; Jäkle, F. *Chem.−Eur. J.* **2008**, *14*, 444−458. (b) Venkatasubbaiah, K.; Pakkirisamy, T.; Lalancette, R. A.; Jäkle, F. *Dalton Trans.*, in press.

(16) Acetonitrile does not significantly bind to **3** at RT; see ref 14.

(17) Scheibitz, M.; Bolte, M.; Bats, J. W.; Lerner, H.-W.; Nowik, I.; Herber, R. H.; Krapp, A.; Lein, M.; Holthausen, M.; Wagner, M. *Chem.−Eur. J.* **2005**, *11*, 584–603.

(18) Scheibitz, M.; Heilmann, J. B.; Winter, R. F.; Bolte, M.; Bats, J. W.; Wagner, M. *Dalton Trans.* **2005**, 159–170.

(19) Metz, M. V.; Schwartz, D. J.; Stern, C. L.; Marks, T. J.; Nickias, P. N. *Organometallics* **2002**, *21*, 4159–4168.

(20) Soriano-Garcia, M.; Toscano, A.; Lopez, T.; Campero-Celis, A. *J. Crystallogr. Spectrosc. Res.* **1987**, *17*, 719–728.

(21) Lesley, M. J. G.; Woodward, A.; Taylor, N. J.; Marder, T. B.; Cazenobe, I.; Ledoux, I.; Zyss, J.; Thornton, A.; Bruce, D. W.; Kakkar, A. K. *Chem. Mater.* **1998**, *10*, 1355.

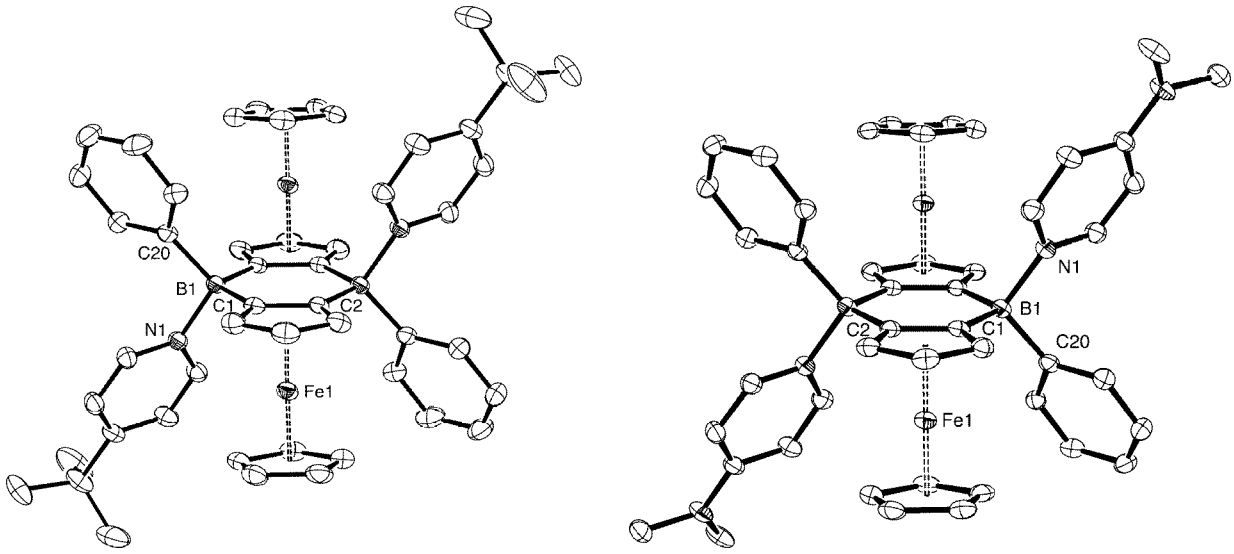

Figure 1. Molecular structures of *trans*-**5b** (left) and *trans*-**5c** (right) with thermal ellipsoids at the 50% probability level; cocrystallized solvent molecules ($CHCl_3$ for *trans*-**5c**) and hydrogen atoms are omitted for clarity.

Table 1. Selected Interatomic Distances (Å) and Angles (deg) for 4b, *trans*-5b, and *trans*-5c in Comparison to Those of 3

		4b			
	3	for B2	for B1	*trans*-**5b**	*trans*-**5c**
B−C_{Cp}	1.546(2)	1.550(7)	1.610(7)	1.610(4)	1.619(4)
	1.546(2)	1.553(7)	1.608(6)	1.602(4)	1.616(4)
B−C_{Ph}	1.564(2)	1.570(7)	1.609(7)	1.628(5)	1.628(4)
B−N			1.659(6)	1.652(3)	1.640(4)
Fe···B	3.032	2.920	3.298	3.408	3.371
Fe···B*	2.957	3.076	3.414	3.376	3.396
B···B*	3.103	3.198		3.278	3.296
Fe···Fe*	5.123	5.445		5.940	5.910
C_{Cp}−B−C_{Cp}	115.8(1)	115.6(4)	110.1(4)	110.1(2)	109.6(2)
$Cp_{Centroid}$−C−B	167.9	161.7	177.14[a]	174.8[a]	177.3[a]
	164.4	168.9	174.19[a]	176.3[a]	175.9[a]
Cp//C_4B_2	15.9	[b]		5.5	4.2
staggering angle	11.4	23/24		33	36.1
Cp_{cent}−Cp_{cent}	3.308	3.308/3.326		3.316	3.316
Cp//Cp tilt	1.2	0.5/4.3		5.4	6.1

[a] The boron atom is above the plane of the respective substituted Cp rings (exoside). [b] The dihedral angles, which were determined to be 8.3° and 14.8°, are not meaningful because the C_4B_2 ring is strongly puckered.

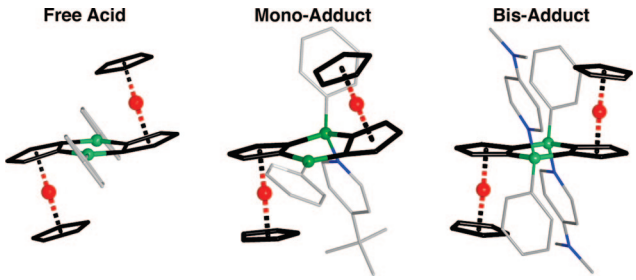

Figure 2. Illustration of the geometric changes to the diboradiferrocene framework upon pyridine binding to **3**.

We obtained orange single crystals of the mono-adduct **4b** from a 1:1 mixture of **3**/*t*Bupy in CH_2Cl_2 that was layered with hexanes and subsequently kept at −35 °C. An X-ray structure plot of **4b** is shown in Figure 3, and selected bond lengths and angles are provided in Table 1. The molecular structure confirms the formation of a 1:1 complex, which consists of one tricoordinate Lewis acidic borane moiety and one coordinatively saturated tetracoordinate boron center. Thus, **4b** shows features reminiscent of both the free Lewis acid **3** and the complex *trans*-

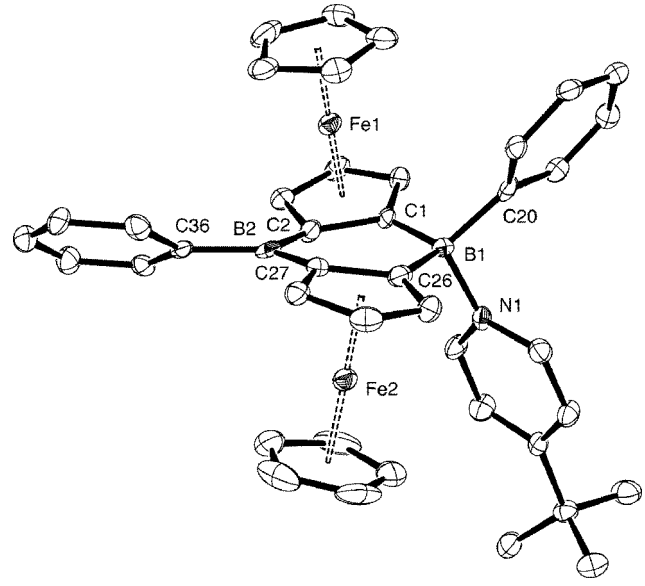

Figure 3. Molecular structure of **4b** with thermal ellipsoids at the 50% probability level; hydrogen atoms are omitted for clarity. Fe1···B1 = 3.298; Fe1···B2 = 2.920, Fe2···B1 = 3.414; Fe2···B2 = 3.076 Å.

5b. As observed also in the free acid **3**, both ferrocene moieties are strongly tilted toward the free triarylborane group due to a delocalized iron−boron interaction. However, they are not tilted toward the boron that is ligated by the pyridine. As a consequence, the Fe···B distances are considerable shorter for the tricoordinate boron (Fe1···B2 = 2.920, Fe2···B2 = 3.076 Å) than for the tetracoordinate boron (Fe1···B1 = 3.298, Fe2···B1 = 3.414 Å). Additional plots are provided in the Supporting Information (Figure S8) to further illustrate these unusual geometric features of **4b**. Another result of these effects is that the central C_4B_2 ring is strongly puckered, which stands in contrast to the only slightly puckered structure of the 1:1 acetonitrile adduct of the perfluorodiboraanthracene derivative [$C_6F_4(\mu$-$BC_6F_5)_2C_6F_4$] reported by Marks.[19] In addition, the dihedral angle between the two substituted Cp rings in **4b** is much larger at 19.7° than that for the two C_6F_4 rings in Marks's complex (9.9(3)°). The boron−carbon bond lengths at the coordinated boron center (B1) are elongated compared to those

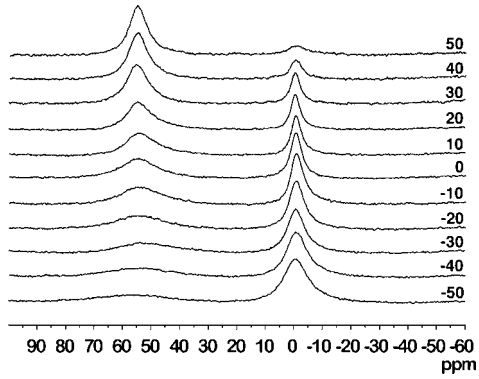

Figure 4. VT ^{11}B NMR spectra for complexation of **3** with 1 equiv of 4-*tert*-butylpyridine in $CDCl_3$ (25 mM).

of the free Lewis acid site (B2) due to the change in the hybridization resulting from expansion of the coordination sphere to a tetrahedral environment for B1.[19] The B−N distance of 1.659(6) Å for **4b** is similar to those of the bis-adducts *trans*-**5b** and *trans*-**5c** (1.652(3) and 1.640(4) Å) and long in comparison to that of the adduct $B(C_6F_5)_3 \cdot$DMAP.[21]

IR spectroscopy provides another potentially useful tool to further study the complex formation through analysis of the B−N stretching modes. Several bands are observed in the region typical of B−N stretching vibrations (ca. 1150 to 1050 cm^{-1})[7] at 1103, 1072, 1048, 1032 cm^{-1} for *trans*-**5b** and at 1105, 1078, 1034 cm^{-1} for *trans*-**5c**; similar modes are also found for the mono-adducts **4b** at 1105, 1072, 1046 cm^{-1} and **4c** at 1104, 1081, 1050, 1032 cm^{-1}. However, the free acid **3** also shows a number of bands in this region (1107, 1082, 1041 cm^{-1}). Thus, a conclusive assignment as to which of the bands may represent the B−N stretch was not possible. More definite evidence of nucleophile binding is provided from inspection of the region for the C═C/C═N ligand stretching modes around 1450 to 1650 cm^{-1}, where the free acid **3** shows only very weak IR modes. Intense bands are found for *trans*-**5c** at 1629 and 1542 cm^{-1} and for **4c** at 1632 and 1543 cm^{-1}, which are similar to those reported for $FcBMe_2$(DMAP)[7] (1636, 1544 cm^{-1}) and strongly shifted to higher energy in comparison to the free ligand vibrations (1603, 1537, 1519 cm^{-1}). The spectra of *trans*-**5b** and **4b** feature prominent bands at 1628, 1504 cm^{-1} and 1627, 1503 cm^{-1}, respectively, which are similar to those for $FcBMe_2$(picoline)[7] (1628, 1507 cm^{-1}).

Solution Binding Studies: Observation of Mono-adducts in Solution. While the bis-adducts **5b** and **5c** are readily isolated as solid materials, their formation in solution is not favorable. Therefore, we will first discuss the properties of the mono-adducts **4b** and **4c**, which are more readily observed in solution. They were generated by mixing a $CDCl_3$ solution of **3** in a 1:1 molar ratio with *t*Bupy and DMAP, respectively, and the resulting solutions were subjected to VT NMR spectroscopic analysis.

The ^{11}B NMR spectrum of **4b** in $CDCl_3$ at −50 °C shows two distinct resonances of approximately equal intensity at ca. 54 and −0.2 ppm, consistent with one boron center that is coordinated by pyridine and one tricoordinated borane moiety (Figure 4). As expected, the resonance at −0.2 ppm for the tetracoordinate boron is considerably sharper than that for the tricoordinate borane moiety. The ^{11}B NMR spectra undergo distinct changes with temperature as shown for **4b** in Figure 4. The signal due to the tetracoordinate boron moiety becomes smaller as the temperature is raised and almost disappears at +50 °C. This indicates that at higher temperature the equilibrium is shifted toward the free acid **3**. A separate peak for the precursor **3** is not observed, but this is not surprising since the signal is very broad and the peaks for **3** and the tricoordinate boron atom of **4b** are expected to appear in the same region and hence to overlap. Similar results are obtained for **4c**, except that the resonance for the tetracoordinate boron, which is found at −1.9 ppm, is relatively more intense, indicating stronger binding of DMAP. At −50 °C only one signal could be identified at −1.9 ppm, presumably due to extreme broadening of the second resonance.

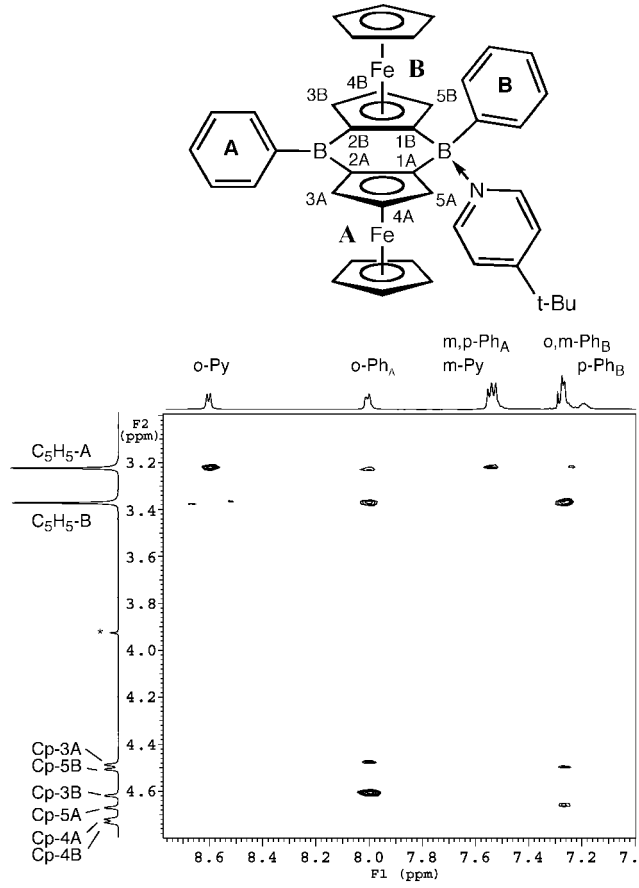

Figure 5. Aromatic/Cp region of the NOESY NMR spectrum of **4b** in $CDCl_3$ at −50 °C (20 mM); a small signal due to a trace amount of **3** is marked with an asterisk.

The ^{1}H NMR spectra are strongly broadened at RT, and especially for **4b** the signals are close to those of the free acid **3**. However, at −50 °C well-resolved signals are observed, which can be assigned to the mono-adducts **4b** and **4c**. The ^{1}H NMR data are discussed here for **4b**; very similar data were obtained also for **4c**. The chemically nonequivalent Ph groups give rise to two separate sets of signals. For **4b**, one set with a distinct doublet for the *ortho*-protons at δ 7.98 is attributed to the Ph group (A) attached to the tricoordinate boron, while an upfield shift of the *ortho*-protons of the Ph ring (B) to δ 7.25 is observed upon pyridine coordination (see *F*1 dimension in Figure 5). This assignment is further confirmed by the observation of NOE peaks between the pyridyl moiety and the Ph group B, but not the Ph group A (not shown). Two sets of signals are also found for the ferrocene moieties, because one of the ferrocene moieties (A) is positioned beside the *t*BuPy ring and the other one (B) next to the Ph group B. The individual resonances in the Cp region at δ 4.69, 4.65, 4.43, 3.21 are assigned to the ferrocene moiety (A) and the signals at δ 4.71, 4.57, 4.45, 3.35 to the ferrocene moiety (B) based on H,H-COSY

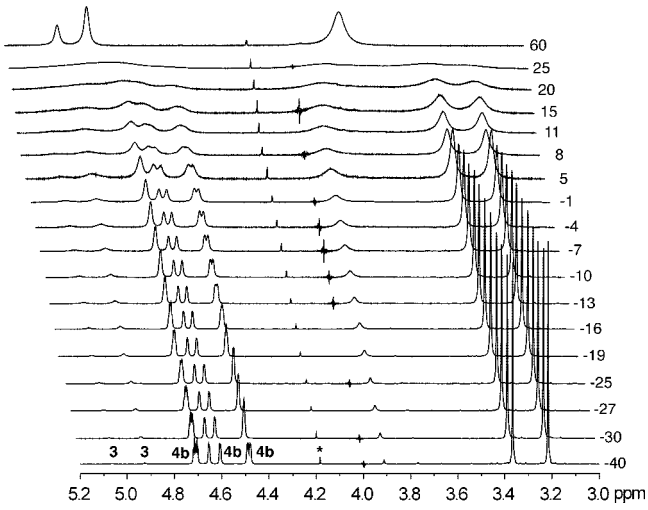

Figure 6. Cp region of the VT ^{1}H NMR spectra for the complexation of **3** with 1 equiv of *tert*-butylpyridine in $CDCl_3$ (20 mM). A trace amount of ferrocene is marked with an astersisk. For detailed assignments of the resonances of complex **4b** see Figure 5.

correlation and NOE spectroscopy (Figure 5). The *ortho*-protons of the Ph ring B display NOE peaks with Cp-5A and Cp-5B, whereas those of the Ph ring A show cross-peaks with Cp-3A and Cp-3B. Most importantly, a distinct cross-peak of the *ortho*-*t*BuPy protons at δ 8.58 with the signal for the free Cp ring C_5H_5-A at 3.21 ppm allows the assignment of that ferrocene moiety as being adjacent to the pyridine group. A cross-peak of the *ortho*-protons of the phenyl ring B with the resonance for the free Cp ring B at δ 3.35 is then consistent with the ferrocenyl group B in a position next to the phenyl ring B. The assignment of the free Cp rings is further confirmed by a weak cross-peak between the Cp-5B resonance at δ 4.71 and the signal for the free Cp ring B at δ 3.35 (not shown).

The variable-temperature ^{1}H NMR spectra over the range from −40 to +60 °C are displayed in Figure 6. At low temperature the mono-adduct **4b** is the dominant species, as already noted above, but the signals for the free acid **3** become relatively more intense as the temperature is gradually increased. At room temperature, the signals are strongly broadened, and at +60 °C only one set of broad resonances is found that is very close to the shifts for the free acid **3**. In this temperature range ligand dissociation becomes very prominent and well-defined coalescence temperatures could not be determined. However, analysis of the signal intensities over the range from −40 to +25 °C allows for construction of a van't Hoff plot for the equilibrium between **3** and **4b**. A linear plot of the equilibrium constant ln K_1 versus $1/T$ with good correlation of $R^2 = 0.9978$ is obtained (see Figure S1 in the Supporting Information). The enthalpy change for the *tert*-butylpyridine binding was determined to be $\Delta H_{ass} = -63.8 \pm 1.7$ kJ mol^{-1} and the entropy change to $\Delta S_{ass} = -174 \pm 7$ J mol^{-1} K^{-1}. A binding constant of log $K_1(298) = 2.1 \pm 0.1$ is deduced.

Initial NMR screening indicated that DMAP is much more strongly bound than *t*Bupy and the 1:1 complex with DMAP is the dominant species even at ambient temperature. A set of small signals for **3** indicates a certain degree of ligand dissociation also for **4c**, but the signals are strongly broadened and accurate signal integration in the temperature range from +20 to +60 °C was not possible. Hence, we decided to use UV−visible spectral titrations, which provide good sensitivity at far lower concentrations than those typically used for ^{1}H NMR analysis. A plot for the titration of **3** with DMAP is shown in Figure 7. Under

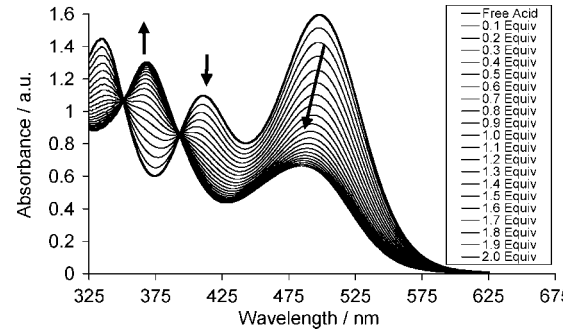

Figure 7. UV−visible titration for the complexation of **3** with 4-dimethylaminopyridine in CH_2Cl_2 (for **3**, $c = 2.99 \times 10^{-4}$ M).

the conditions employed, only the mono-adduct **4c** is formed without any significant amount of **5c**. Fitting of the spectral data to a 1:1 binding process by analysis of 248 different wavelengths using the program Hyperquad gave a binding constant of log $K_1 = 4.28(1)$. A similar UV−visible titration with *t*Bupy gave log $K_1 = 2.49(1)$ (see Supporting Information), which is in reasonably good agreement with the NMR results described above. Thus, binding of the first molecule of DMAP to **3** is about 2 orders of magnitude stronger than that of *t*Bupy.

Analysis of the spectral titration curves also allows the prediction of the UV−visible spectra of the mono-adducts **4b** and **4c**. The calculated data are shown in comparison to the spectrum of the free acid in Figure S4 of the Supporting Information. The intense low-energy absorption of **3** at 498 nm ($\varepsilon = 5340$ M^{-1} cm^{-1}) experiences a hypsochromic shift upon pyridine binding, and the intensity is strongly diminished. Absorption maxima of 475 nm ($\varepsilon = 2230$ M^{-1} cm^{-1}) and 476 nm ($\varepsilon = 1820$ M^{-1} cm^{-1}) are determined for **4b** and **4c**, respectively.

Observation of the Bis-adducts in Solution. Formation of the bis-adducts **5** from **3** and 2 equiv of base was not observed in $CDCl_3$ at room temperature, and only small amounts of the DMAP adduct **5c** were formed at −50 °C. The bis-adduct **5a** was, however, detected at low temperature in neat d_5-pyridine, and **5c** was readily observed in $CDCl_3$ in the presence of a 5-fold excess of DMAP as described in the following.

The ^{11}B NMR of **3** in neat d_5-pyridine revealed two distinct signals of similar intensity at RT, consistent with the expected structure of monocomplexed **4a** described above (Figure 8). When the temperature is gradually lowered to −50 °C, the signal at ca. 55 ppm further broadens and can eventually not be resolved. This suggests that the equilibrium is shifted toward the doubly complexed species **5a**. However, the observation that the ^{11}B NMR signal at ca. 0 ppm remains very broad indicates that **5a** is still in dynamic exchange with a smaller amount of **4a**, which is not detectable. Similar ^{11}B NMR data were obtained when **3** was examined in the presence of a 5-fold excess of DMAP in $CDCl_3$ solution.

The low-temperature ^{1}H NMR spectrum of **5a** in d_5-pyridine at −50 °C (Figure 9) shows two sets of resonances in the Cp region that can be assigned to the *cis*- and *trans*-isomers of **5a**. The individual assignments were further confirmed by 2D NMR spectroscopy, and the ratio of *cis*-**5a**:*trans*-**5a** was determined by ^{1}H NMR integration to be 1:1.5. Similar patterns were observed for **5c**, which was detected at −50 °C upon dissolution of **3** in the presence of a 5-fold excess of DMAP in $CDCl_3$ (0.023 M in **3**). The ratio of *cis*-**5c**:*trans*-**5c** was determined to be 1:4, and the ratio of **5c**:**4c** at that temperature was 2.7:1 on the basis of ^{1}H NMR integration.

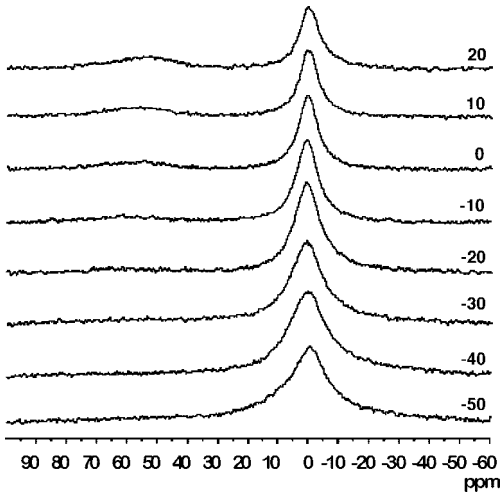

Figure 8. VT ^{11}B NMR spectra of **4a/5a** in d_5-pyridine (20 mM).

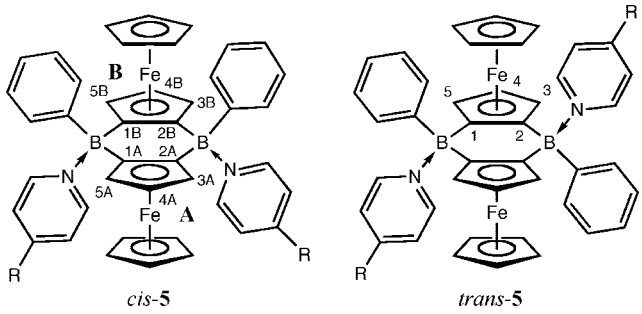

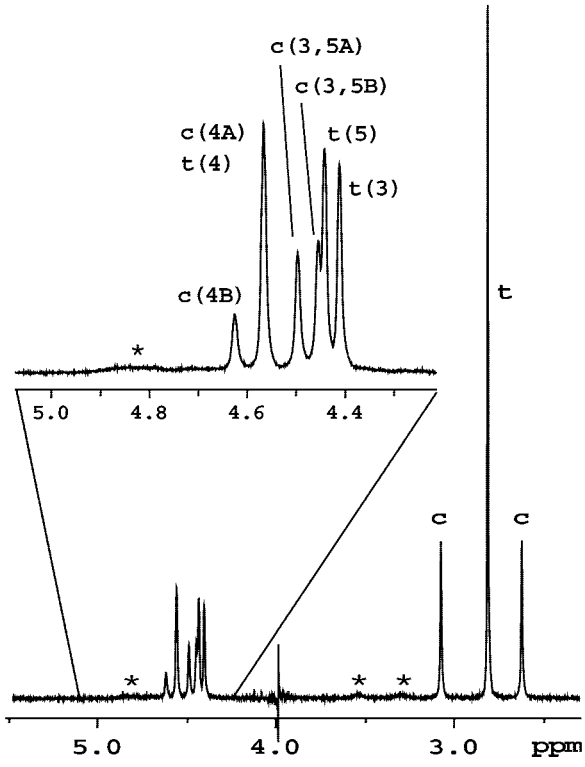

Figure 9. Cp region of the ^{1}H NMR spectrum of **3** in d_5-pyridine at −50 °C (20 mM). Labeling: c corresponds to *cis*-**5a**; t corresponds to *trans*-**5a**; * corresponds to a small amount of the mono-adduct **4a**.

For both compounds, the *cis*-isomer features a mirror plane that intersects the two ferrocene moieties and renders the Cp-3 and Cp-5 protons equivalent. However, the individual ferrocene moieties are not equivalent, because one ferrocene moiety (A) is flanked by two pyridine rings, while the other one (B) is close to two phenyl groups. Consequently, two sets of signals are observed for the free Cp rings and also for the Cp-4 and Cp-3,5 protons. In contrast, the ferrocene moieties are equivalent in the *trans*-isomer, which features an inversion center. Interesting to point out is the unusually strong upfield shift of the resonances for the free Cp rings (*cis*-**5a**, δ 3.08, 2.63/*trans*-**5a**, δ 2.82; *cis*-**5c**, δ 2.73, 2.52/*trans*-**5c**, δ 2.62), which is attributed to the ring current effect of the adjacent phenyl and pyridyl substituents on boron.

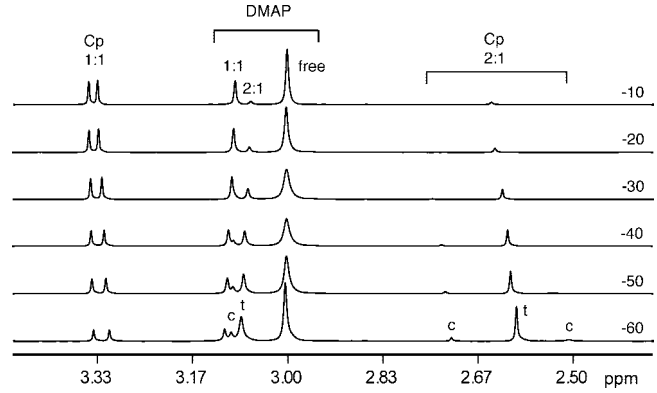

Figure 10. Variable-temperature ^{1}H NMR spectra of a 1:5 mixture of **3**/4-dimethylaminopyridine (DMAP) in $CDCl_3$ (0.023 M in **3**). Only the region featuring the Me groups of the DMAP and the unsubstituted Cp signals is shown. Labeling: "c" corresponds to *cis*-**5c**; "t" corresponds to *trans*-**5c**; "free" denotes the signal due to excess DMAP.

Thermodynamic data for the binding of the second molecule of DMAP to **3** were obtained by ^{1}H NMR analysis of a 1:5 mixture of **3**/DMAP at variable temperatures (Figure 10). Under the conditions applied the concentration of **3** is negligible so that only the equilibrium between **4c** and **5c** needs to be considered. Van't Hoff analysis using integration of the signals for the free Cp rings of **4c** and **5c** at variable temperatures gave a linear plot with a correlation of $R^2 = 0.9912$. The binding enthalpy was determined from the slope to be $\Delta H_{ass} = -44.5 \pm 3.4$ kJ mol^{-1}, and the entropy term was determined to be $\Delta S_{ass} = -171 \pm 14$ J mol^{-1} K^{-1}. The stepwise binding constant at 298 K was calculated to be log $K_2(298) = -1.1 \pm 0.1$ (log $K_2(223) = +1.5 \pm 1$), which shows that binding of the second DMAP molecule is only favorable at low temperature and by more than 5 orders of magnitude weaker than the first binding process.

Conclusions

With pyridine derivatives as the Lewis base the bifunctional Lewis acid **3** forms isolable complexes, in which either one or both Lewis acidic boron centers are coordinated. Single-crystal X-ray diffraction data of the 1:1 and 1:2 adducts reveal pronounced structural changes of the molecular framework upon pyridine binding. The delocalized interaction with the electron-rich ferrocene moieties, which is responsible for tilting of the ferrocene moieties toward boron in the free acid, is intercepted by the tetracoordination of boron. In the case of the mono-adduct a strongly puckered central C_4B_2 ring results because one of the boron atoms is able to interact with the ferrocene moieties while the empty p orbital of the other one is engaging in a donor−acceptor interaction with the pyridine nitrogen. Binding

of the second pyridine leads to the more symmetric structure of compounds **5**. However, the latter show features indicative of increased steric crowding. For instance, the ferrocene moieties are bent away from the boron centers, as evident from the position of the boron atoms above the planes of the substituted Cp rings. Moreover, the Cp rings of the individual ferrocene moieties are tilted by about 5−6°, opening up the ferrocenes toward the dibora-bridge. Consistent with increased steric strain in **5** is the facile pyridine dissociation from the bis-adducts in solution. This results in a very small binding constant determined for the coordination of the second relative to the first DMAP molecule, and hence an unusually pronounced negative binding cooperativity effect.

Experimental Section

Materials and General Methods. Pyridine, 4-*tert*-butylpyridine (*t*Bupy), and 4-dimethylaminopyridine (DMAP) were purchased from Acros. All reactions and manipulations were carried out under an atmosphere of prepurified nitrogen using either Schlenk techniques or an inert-atmosphere glovebox (Innovative Technologies). Hydrocarbon and chlorinated solvents were purified using a solvent purification system (Innovative Technologies), and the chlorinated solvents were subsequently degassed via several freeze−pump−thaw cycles.

The 499.9 MHz ^{1}H NMR, 125.7 MHz ^{13}C NMR, and 160.3 ^{11}B NMR spectra were recorded on a Varian INOVA NMR spectrometer (Varian Inc., Palo Alto, CA) equipped with a boron-free 5 mm dual broadband gradient probe (Nalorac, Varian Inc., Martinez, CA). All solution ^{1}H and ^{13}C NMR spectra were referenced internally to the solvent signals, and ^{11}B NMR spectra were referenced externally to $BF_3 \cdot Et_2O$ in C_6D_6 ($\delta = 0$).

Two-dimensional proton correlation spectroscopy, COSY,[22] proton NOE spectroscopy, NOESY,[23] and one-bond proton−carbon correlation spectroscopy, HMQC,[24] measurements were recorded in the absolute value mode (COSY) or the phase-sensitive mode (NOESY, HMQC) by employing the TPPI improvement[25] of the States−Haberkorn−Ruben hypercomplex method.[26] Selection of desirable coherences and artifact suppression were accomplished by z-gradients (COSY, echo N-type coherence selection[27]) or phase cycles of 32 (NOESY) or 16 (HMQC) steps. The NOESY data set was acquired using a 400 ms mixing time. The HMQC pulse sequence included the BIRD filter to suppress signals from C12-attached protons[28] and C13-decoupling during proton acquisition, using a 3.6 kHz field strength and the GARP decoupling scheme.[29] Typically, 256 t1 increments of 2000 complex data points over 5.5 kHz (proton) and 22.5 kHz (carbon) spectral widths were collected with 1 (COSY), 32 (NOESY), or 16 (HMQC) scans per t1 increment, preceded by 16 or 32 dummy scans, and a relaxation delay of 2 s. Baseline distortion was addressed by properly adjusting the sampling delay and the signal phase.[30] Data sets were processed on a Sun Blade 100 workstation (Sun Microsystems Inc., Palo Alto, CA) using the VNMR software package (Varian Inc., Palo Alto, CA). In order to decrease t1 ridges arising from incorrect treatment of the first data point in the discreet Fourier transform (FT) algorithm, the spectrum corresponding to the first t1 value was divided by 2 prior to FT along t1.[31] Shifted (COSY) or unshifted (NOESY, HMQC) Gaussian window functions were used in both dimensions. Data sets were zero-filled in the t1 dimension yielding 1000 × 1000 final matrices that have not been symmetrized.

UV−visible absorption data were acquired on a Varian Cary 500 UV−vis/NIR spectrophotometer. Solutions were prepared using a microbalance (±0.1 mg) and volumetric glassware and then charged into quartz cuvettes with sealing screw caps (Starna) inside the glovebox. The titrations of **3** with *t*Bupy and DMAP were performed by sequential addition of a stock solution of the pyridine derivative in CH_2Cl_2 to a solution of **3** in CH_2Cl_2 in a Quartz cuvette using a microliter syringe. The binding constants were determined with the Hyperquad program by assuming a 1:1 binding process (justified on the basis of the NMR studies) and using 32 titration points and 282 different wavelengths spanning a range from ca. 315 to 609 nm.

IR spectra were obtained on a Nicolet IR-200 spectrometer. All samples were prepared as KBr pellets. Elemental analyses were performed by Quantitative Technologies Inc., Whitehouse, NJ.

Details of the X-ray diffraction experiments and crystal structure refinements for **4b**, *trans*-**5b**, and *trans*-**5c** are provided in Table 2. Data were collected on Bruker SMART APEX CCD diffractrometers using Cu Kα (1.54178 Å) or Mo Kα (0.71073 Å) radiation. A SADABS[32] absorption correction was applied. The structures were solved using direct methods, completed by subsequent difference Fourier syntheses and refined by full matrix least-squares procedures on F^2. All non-hydrogen atoms were refined with anisotropic displacement coefficients. The H atoms were placed at calculated positions and were refined as riding atoms. All software and source scattering factors are contained in the SHELXTL program package.[33] Crystallographic data for the structures of **4b**, *trans*-**5b**, and *trans*-**5c** have been deposited with the Cambridge Crystallographic Data Center as supplementary publication nos. CCDC-678401, CCDC-275646, and CCDC-678402, respectively. Copies of the data can be obtained free of charge on application to CCDC, 12 Union Road, Cambridge CB21EZ, UK (fax: (+44) 1223-336-033; e-mail: deposit@ccdc.cam.ac.uk).

Complexation of 3 with 1 equiv of 4-*tert*-Butylpyridine: Synthesis of 4b. To a solution of **3** (13.9 mg, 25 μmol) in CH_2Cl_2 (3 mL) was added *t*Bupy (5.2 mg, 38 μmol) in CH_2Cl_2 (2 mL) at room temperature, and the mixture was stirred for 1 h. The reaction solution was layered with hexanes and kept for crystallization for 2 days at −35 °C. The product was isolated as orange block-like crystals. Yield: 14.1 mg (82%). IR (cm^{-1}): 3061, 2967, 1627, 1503, 1428, 1406, 1286, 1192, 1104, 1072, 1045, 812, 736, 707, 570, 482. Anal. Calcd for ($C_{41}H_{39}B_2Fe_2N$): C 72.51 H 5.78 N 2.06. Found: C 72.14 H 5.82 N 2.02.

Low-Temperature NMR Characterization of 4b. Complex **4b** was generated by mixing **3** with *t*Bupy in $CDCl_3$ in a 1:1 molar ratio and studied by VT NMR spectroscopy. At room temperature the equilibrium was found to be far on the side of the free acid (**3**): ^{1}H NMR (500 MHz, $CDCl_3$, 25 °C) δ 8.56 (br, 2H, *o*-*t*Bupy), 7.96 (br, 4H, *o*-Ph), 7.49 (b m, 8H, *m*-*t*Bupy, *m*,*p*-Ph), 5.04 (b, 2H, 4-Cp), 4.92 (b, 4H, 3,5-Cp), 3.90 (b, 10H, free Cp), 1.37 (s, 9H, Me); ^{11}B NMR (160 MHz, $CDCl_3$, 25 °C) δ 55.5 ($w_{1/2}$ = 1300 Hz) and −0.7 ($w_{1/2}$ = 320 Hz) (ratio 27:1). At low temperature, the 1:1 adduct

(22) (a) Aue, W. P.; Bartholdi, E.; Ernst, R. R. *J. Chem. Phys.* **1976**, *64*, 2229. (b) Bax, A.; Freeman, R. *J. Magn. Reson.* **1981**, *44*, 542.
(23) (a) Muller, L. *J. Am. Chem. Soc.* **1979**, *101*, 4481. (b) Jeener, J.; Meier, B. H.; Bachmann, P.; Ernst, R. R. *J. Chem. Phys.* **1979**, *71*, 4546.
(24) (a) Macura, S.; Ernst, R. R. *Mol. Phys.* **1980**, *41*, 95–117. (b) Bax, A.; Subramanian, S. *J. Magn. Reson.* **1986**, *67*, 565.
(25) (a) Redfield, A. G.; Kunz, S. D. *J. Magn. Reson.* **1975**, *19*, 250–254. (b) Marion, D.; Wüthrich, K. *Biochem. Biophys. Res. Commun.* **1983**, *113*, 967.
(26) States, D. J.; Haberkorn, R. A.; Ruben, D. J. *J. Magn. Reson.* **1982**, *48*, 286–292.
(27) von Kienlin, M.; Moonen, C. T. W.; van der Toorn, A.; van Zijl, P. C. M. *J. Magn. Reson.* **1991**, *93*, 423.
(28) Garbow, J. R.; Weitekamp, D. P.; Pines, A. *Chem. Phys. Lett.* **1982**, *93*, 504.
(29) Shaka, A. J.; Barker, P. B.; Freeman, R. *J. Magn. Reson.* **1985**, *64*, 547.
(30) Hoult, D. I.; Chen, C. N.; Eden, H.; Eden, M. *J. Magn. Reson.* **1983**, *51*, 110.
(31) Otting, G.; Widmer, H.; Wagner, G.; Wüthrich, K. *J. Magn. Reson.* **1986**, *66*, 187–193.
(32) Sheldrick, G. M. *SADABS*, Version 2. Multi-Scan Absorption Correction Program; University of Göttingen: Germany, 2001.
(33) Sheldrick, G. M. *SHELXTL*, Version 6.14; Bruker AXS Inc.: Madison, WI, 2004.

Table 2. Details of X-ray Structure Determinations

	4b	***trans*-5b**	***trans*-5c**
empirical formula	$C_{41}H_{39}B_2Fe_2N$	$C_{50}H_{52}B_2Fe_2N_2$	$C_{48}H_{48}B_2Fe_2N_4Cl_6$
MW	679.05	814.26	1026.92
T, K	100(2)	213(2)	100(2)
wavelength, Å	1.54178	0.71073	1.54178
cryst syst	orthorhombic	monoclinic	triclinic
space group	*Pna*2(1)	*C*2/*c*	$P\bar{1}$
a, Å	9.5763(6)	28.2223(18)	9.9484(4)
b, Å	19.3314(12)	8.3188(5)	10.4634(4)
c, Å	17.4565(9)	21.8954(14)	11.6449(4)
α, deg	90	90	70.117(2)
β, deg	90	127.6860(10)	78.568(3)
γ, deg	90	90	84.032(3)
V, Å^3	3231.6(3)	4068.1(4)	1116.41(7)
Z	4	4	1
ρ_{calc}, g cm^{-3}	1.396	1.527	1.527
μ(Cu/Mo$_{K\alpha}$), mm^{-1}	7.423	0.751	8.828
F(000)	1416	1712	528
cryst size, mm	0.24 × 0.19 × 0.17	0.30 × 0.20 × 0.15	0.25 × 0.18 × 0.12
θ range, deg	3.41 − 67.31	1.82 − 28.22	4.10 − 67.82
limiting indices	$-11 \le h \le 11$	$-34 \le h \le 36$	$-8 \le h \le 11$
	$-21 \le k \le 22$	$-11 \le k \le 10$	$-12 \le k \le 12$
	$-20 \le l \le 20$	$-28 \le 1 \le 27$	$-13 \le l \le 13$
no. of reflns collected	16 928	14 480	10 152
no. of indep reflns	5309 [*R*(int) = 0.1105]	4785 [*R*(int) = 0.0362]	3656 [*R*(int) = 0.0275]
absorp corr		semiempirical from equivalents	
refinement method		full-matrix least-squares on F^2	
no. of data/restraints/params	5309/1/419	4785/0/253	3656/0/282
GOF on F^2	0.935	1.150	1.078
final *R* indices	R1 = 0.0458	R1 = 0.0527	R1 = 0.0459
$[I > 2\sigma(I)]^a$	wR2 = 0.0828	wR2 = 0.1257	wR2 = 0.1159
R indices (all data)^a	R1 = 0.0810	R1 = 0.0610	R1 = 0.0459
	wR2 = 0.0953	wR2 = 0.1303	wR2 = 0.1181
Flack param	0.003(5)		
peak$_{max}$/hole$_{min}$ (e Å^{-3})	0.656/−0.382	0.517/−0.423	0.744/−0.383

^{a} $R1 = \sum||F_o| - |F_c||/\sum|F_o|$; $wR2 = \{\sum[w(F_o^2 - F_c^2)^2]/\sum[w(F_o^2)^2]\}^{1/2}$.

was observed. Assignments are based on 2D NMR correlations (COSY, HMQC, NOESY). For **4b** (20 mM solution in $CDCl_3$): ^{1}H NMR (500 MHz, $CDCl_3$, −50 °C) δ 8.58 (d, J = 6.5 Hz, 2H, *o*-*t*Bupy), 7.99−7.97 (m, 2H, *o*-Ph$_A$), 7.53−7.49 (m, 5H, *p*-Ph$_A$, *m*-Ph$_A$ and *m*-*t*Bupy), 7.25−7.23 (m, 4H, *o*,*m*-Ph$_B$), 7.18 (m, 1H, *p*-Ph$_B$), 4.71 (pst, J = 2 Hz, 1H, 4-Cp$_B$), 4.69 (pst, J = 2 Hz, 1H, 4-Cp$_A$), 4.65 (nr, 1H, 5-Cp$_A$), 4.57 (nr, 1H, 3-Cp$_B$), 4.45 (nr, 1H, 5-Cp$_B$), 4.43 (nr, 1H, 3-Cp$_A$), 3.35 (s, 5H, Cp$_B$), 3.21 (s, 5H, Cp$_A$), 1.35 (s, 9H, *t*Bu); ^{13}C NMR (125.69 MHz, $CDCl_3$, −50 °C) δ 164.8 (*i*-*t*Bupy), 146.3 (*o*-*t*Bupy), 144.8 (*i*-Ph$_A$), 133.2 (*o*-Ph$_B$), 133.0 (*o*-Ph$_A$), 128.0 (*p*-Ph$_A$), 127.4 (*m*-Ph$_A$), 126.7 (*m*-Ph$_B$), 124.8 (*m*-Ph$_B$), 121.6 (*m*-*t*Bupy), 80.2 (*i*-Cp$_A$, *i*-Cp$_B$), 78.9 (3-Cp$_A$), 78.1 (5-Cp$_A$, 5-Cp$_B$), 76.5 (5-Cp$_B$), 76.2 (4-Cp$_A$), 75.8 (5-Cp$_A$), 74.8 (4-Cp$_B$, 3-Cp$_A$), 69.7 (Cp$_B$), 68.4 (Cp$_A$), 35.6 (−*C*Me$_3$), 30.2 (−C*Me*$_3$); ^{11}B NMR (160 MHz, $CDCl_3$, −50 °C) δ 54 ($w_{1/2}$ = 4800) and −0.2 ($w_{1/2}$ = 1700).

Complexation of 3 with 1 equiv of 4-Dimethylaminopyridine: Synthesis of 4c. To a solution of **3** (40 mg, 74 μmol) in CH_2Cl_2 (4 mL) was added DMAP (9 mg, 74 μmol) in CH_2Cl_2 (2 mL) at room temperature, and the mixture was stirred for 1 h. The reaction solution was layered with hexanes and kept for crystallization for 2 days at −35 °C. The product was isolated as a reddish crystalline solid. Yield: 39.5 mg (80%). IR (cm^{-1}): 3057, 2923, 1632, 1543, 1393, 128, 1226, 1189, 1104, 1081, 1050, 1032, 816, 717. Anal. Calcd for $(C_{39}H_{36}B_2Fe_2N_2)\cdot(CH_2Cl_2)_{0.2}$: C 68.93 H 5.37 N 4.10. Found: C 68.88 H 5.35 N 4.12 (the sample contained a small amount of residual CH_2Cl_2 according to ^{1}H NMR despite evacuation under high vacuum at 40 °C for 12 h).

Low-Temperature NMR Characterization of 4c. Complex **4c** was generated by mixing **3** with DMAP in $CDCl_3$ in a 1:1 molar ratio and studied by VT NMR spectroscopy. The complex was detected at RT as well as −50 °C; at RT the resonances are broadened and a small amount of free **3** is observed. The assignments are based on an H,H-COSY spectrum and comparison with those of **4b**. For **4c**: ^{1}H NMR (500 MHz, $CDCl_3$, −50 °C) δ 8.15 (d, J = 7.0 Hz, 2H, *o*-DMAP), 8.00 (d, J = 7.0 Hz, 2H, *o*-Ph$_A$), 7.52−7.51 (m, 3H, *p*-Ph$_A$, and *m*-Ph$_A$), 7.27−7.24 (m, 4H, *o*,*m*-Ph$_B$), 7.15 (m, 1H, *p*-Ph$_B$), 6.53 (d, J = 6.5 Hz, 2H, *m*-DMAP), 4.71 (nr, 1H, 4-Cp$_B$), 4.66 (nr, 1H, 4-Cp$_A$), 4.61 (nr, 1H, 5-Cp$_B$), 4.60 (nr, 1H, 3-Cp$_A$), 4.50 (nr, 1H, 5-Cp$_B$), 4.45 (nr, 1H, 3-Cp$_A$), 3.37, 3.34 (s, 5H, Cp$_A$ and s, 5H, Cp$_B$), 3.14 (s, 6H, NMe$_2$); ^{11}B NMR (160 MHz, $CDCl_3$, −50 °C) δ −1.9 ($w_{1/2}$ = 1000 Hz), the signal for the tricoordinate B is broadened beyond detection.

Complexation of 3 with 2 equiv of Pyridine: Synthesis of 5a. Compound **3** (17.1 mg, 31 μmol) was dissolved in pyridine (49 mg, 630 μmol) at RT. After 1 day at −35 °C a crystalline solid was obtained, which was washed with hexanes and dried under high vacuum. Yield for **5a**: 17.5 mg (80%). Anal. Calcd for **5a** ($C_{42}H_{36}B_2Fe_2N_2$): C 71.85 H 5.17 N 3.99. Found: C 71.70 H 5.15 N 3.47. ^{11}B NMR (160 MHz, $CDCl_3$, 25 °C): δ 54.4 ($w_{1/2}$ = 1400 Hz), 0.1 ($w_{1/2}$ = 900 Hz).

Low-Temperature NMR Characterization of 5a. The *cis*- and *trans*-isomers of **5a** were identified at −50 °C in neat d_5-pyridine by 2D NMR spectroscopy (COSY). The ratio of *cis*/*trans*-isomer was found to be 40/60 under these conditions. ^{1}H NMR (500 MHz, C_5D_5N, −50 °C): NMR data for *cis*-**5a**: δ 7.42−7.20 (nr, 10H, Ph), 4.62 (nr, 1H, Cp-4B), 4.56 (nr, 1H, Cp-4A), 4.49 (nr, 2H, Cp-3A/5A), 4.45 (nr, 2H, Cp-3B/5B), 3.08 (s, 5H, C_5H_5-B), 2.63 (s, 5H, C_5H_5-A); NMR data for *trans*-**5a**: δ 7.42−7.20 (m, 10H, Ph), 4.56 (nr, 2H, Cp-4), 4.43, 4.41 (nr, nr, 2H, 2H, Cp-3 and Cp-5), 2.82 (s, 10H, C_5H_5). An additional set of small and very broad signals is assigned to **4a** (δ 8.6, 8.3−7.5, 6.4, 4.9−4.6, 3.55, 3.21).

Complexation of 3 with 2 equiv of 4-*tert*-Butylpyridine: Synthesis of 5b. Neat *t*Bupy (9.9 mg, 73 μmol) was added to a solution of **3** (20.1 mg, 36 μmol) in $CHCl_3$ (10 mL) at RT. After stirring for 3 h the solvent was removed under reduced pressure

and the remaining solid was washed with hexanes. Orange crystals of *trans*-**5b** were obtained by slow evaporation of a solution in $CHCl_3$. Yield: 26.4 mg (88%). ^{1}H NMR (500 MHz, $CDCl_3$, 25 °C): δ 8.56, 7.97, 7.48 and 7.32 (b, 18H, aromatic), 4.75, 4.65, 3.83, 3.41, and 3.24 (b, 16H, Cp), 1.34 (s, 18H, Me). ^{11}B NMR (160 MHz, $CDCl_3$, 20 °C): δ 55.4 ($w_{1/2}$ = 1100 Hz) and −0.4 ($w_{1/2}$ = 550 Hz). IR (cm^{-1}): 3059, 2965, 1628, 1504, 1428, 1277, 1222, 1157, 1103, 1072, 1048, 1035, 999, 834, 814, 773, 738, 713, 572, 501, 479, 463. Anal. Calcd for ($C_{50}H_{52}B_2Fe_2N_2$): C 73.75 H 6.43 N 3.44. Found: C 73.99 H 6.64 N 3.68.

Complexation of 3 with 2 equiv of 4-Dimethylaminopyridine: Synthesis of 5c. To a suspension of **3** (17.5 mg, 32 μmol) in CH_2Cl_2 (3 mL) was added DMAP (8.6 mg, 71 μmol) in CH_2Cl_2 (2 mL) at room temperature, and the mixture was stirred for 2 h. The reaction solution was kept for crystallization for 2 days at −35 °C, and the product was isolated as orange needle-like crystals. Yield: 19.4 mg (77%). A sample of *trans*-**5c** for X-ray diffraction and elemental analysis was obtained by recrystallization from $CHCl_3$ at −35 °C. ^{11}B NMR (160 MHz, $CDCl_3$, 25 °C): δ 54.1 ($w_{1/2}$ = 1600 Hz), −1.8 ($w_{1/2}$ = 480 Hz) (ratio 0.5:1). IR (KBr, cm^{-1}): 3056, 2921, 1629, 1542, 1225, 1148, 1105, 1078, 1034, 808, 719, 708, 478. Anal. Calcd for ($C_{46}H_{46}B_2Fe_2N_4$)($CHCl_3$)$_{2.3}$: C 54.59 H 4.58 N 5.27. Found: C 54.44 H 4.14 N 5.20.

Low-Temperature NMR Characterization of 5c. The low-temperature NMR of a 1:5 mixture of **3**/DMAP in $CDCl_3$ showed signals corresponding to complexes **4c**, **5c**, and free DMAP. The ratio of **5c**:**4c** was determined to be 73:27 based on ^{1}H NMR integration. Both the *cis*- and *trans*-isomers of **5c** (20:80 ratio) were identified. For **5c**: ^{1}H NMR (500 MHz, $CDCl_3$, −50 °C) the signals in the aromatic region could not be assigned; for *cis*-**5c**: δ 4.31 (nr, 1H, Cp-4B), 4.21 (nr, 2H, Cp-3B/5B), 4.16 (nr, 1H, Cp-4A), 4.04 (nr, 2H, Cp-3A/5A), 3.12 (s, 12H, NMe_2), 2.73, 2.52 (s, 5H, C_5H_5-B and s, 5H, C_5H_5-A); for *trans*-**5c**: δ 4.22, 4.12 (nr, nr, 2H, 2H, Cp-3 and Cp-5), 4.08 (nr, 2H, Cp-4), 3.10 (s, 12H, NMe_2), 2.62 (s, 10H, C_5H_5).

Acknowledgment. Acknowledgment is made to the donors of the Petroleum Research Fund, administered by the American Chemical Society, and to the Rutgers University Research Council for support of this research. We thank the National Science Foundation for partial funding of an X-ray diffractometer (NSF-CRIF 0443538). F.J. thanks the Alfred P. Sloan Foundation for a research fellowship and the National Science Foundation for a CAREER award. We are grateful to Dr. Kakalis for acquisition of 2D NMR data.

Supporting Information Available: Crystallographic data for compounds **4b** and *trans*-**5c**, including tables of crystal data, atomic coordinates, bond lengths and angles, and anisotropic thermal parameters; details of the VT NMR studies; details of the UV−visible titration of **3** with *tert*-butylpyridine. This material is available free of charge via the Internet at http://pubs.acs.org.

OM8001608